Observing electron-correlation features in two-photon double ionization of helium

Wei-Chao Jiang,[1,2] Stefan Nagele,[2] and Joachim Burgdörfer[2]
[1]*College of Physics and Energy, Shenzhen University, Shenzhen 518060, China*
[2]*Institute for Theoretical Physics, Vienna University of Technology, Wiedner Hauptstraße 8-10, A-1040 Vienna, Austria, EU*
(Received 21 June 2017; published 27 November 2017)

By numerically solving the time-dependent Schrödinger equation for helium in its full dimensionality, we determine the joint momentum spectrum along the polarization direction $P(k_{1z},k_{2z})$ for two-photon double ionization (TPDI). We identify features uniquely attributable to dynamical correlation effects in the double continuum. We show that some of the correlation signatures persist in integrated measures, in particular the emission asymmetry, that should become accessible with upcoming XUV light sources. We also compare with predictions of analytic models for TPDI which neglect such final-state correlations.

DOI: 10.1103/PhysRevA.96.053422

I. INTRODUCTION

Modern experimental techniques, such as velocity map imaging (VMI [1]) and cold target recoil ion momentum spectroscopy (COLTRIMs [2]), provide direct access to multi-differential information on charged-particle fragmentation patterns following atomic collisions or photoionization. Angle-resolved photoelectron spectra now serve as important tools for accurate studies of laser-atom interactions. The simultaneous determination of the vectorial momenta of ejected electrons and recoil ions allows one to determine the momentum correlation between electrons emitted in multielectron emission events. For example, joint projected momentum spectra along the laser polarization axis $P(k_{1z},k_{2z})$, integrated over all transverse components, have been measured for strong-field double ionization of atoms by near-infrared lasers [3–8]. Recently, the measurement of these joint momentum spectra was extended to wavelengths in the midinfrared [9]. These experimental advances have given rise to a large number of theoretical studies and simulations [10–14]. However, for the very fundamental process of two-photon double ionization (TPDI) of helium by an XUV pulse, such joint momentum spectra are not yet available due to the limited photon flux and resulting low count rates of heretofore available XUV light sources. Nevertheless, the free-electron laser (FEL) source FLASH allowed for the measurement of the momentum-differential He^{2+} recoil ion distribution [15], providing the first indirect information on the joint momentum distribution. Explicit theoretical predictions for $P(k_{1z},k_{2z})$ are, to our knowledge, also missing.

TPDI of helium has attracted significant attention from both the theoretical [16–56] and experimental side [15,57–59]. TPDI of helium is one of the quantum three-body problems that nowadays can be solved, though numerically, yet essentially exactly. With the availability of novel light sources in the EUV and XUV regimes, namely, high-order-harmonic generation (HHG)-based sources for subfemtosecond pulses [58,60,61] and FELs generating trains of pulses of $\sim$10 fs duration [15,57,59], TPDI has become experimentally accessible. For few-photon absorption, perturbation theory can be successfully applied to account for both one-photon double ionization (PDI) and TPDI. Compared to PDI, TPDI is intrinsically more complex. In addition to the initial ground state and the final double continuum state, also the accurate representation of relevant intermediate states is required. Recently, it has been recognized that single-ionization continuum states are the most important intermediate states both in the sequential ($\omega > 54.4$ eV) and nonsequential regimes ($39.5 < \omega < 54.4$ eV) of TPDI [16,22–25,48–51,55]. Exploiting this observation, Ishikawa *et al.* [16], Horner *et al.* [22–25], Førre *et al.* [48,55], and Jiang *et al.* [49–51] have developed closely related simple (semi)analytic models that are capable of predicting the total cross section (or the total double-ionization probability) and the energy spectrum of the two electrons in TPDI. The price to pay for such a simplified treatment is the neglect of dynamical correlation effects in the two-electron continuum from the outset. Amazingly, these simple models have predicted total double-ionization probabilities and energy spectra that are quantitatively comparable to results from the elaborate numerical time-dependent Schrödinger equation (TDSE) methods.

The success of these models originates primarily from two features: within second-order time-dependent perturbation theory, the energies of the initial, intermediate, and final states enter as parameters, which can be accurately accounted for by using input from either accurate time-independent calculations (and, thus, containing so-called static correlations) or from experiment. Moreover, the time ordering of the underlying (non)sequential processes and the spectral broadening due to the transient population of the intermediate states within the ultrashort pulse duration is included in the nested double integral [see Eq. (14) below] [16,22–25], often referred to as a "shape" function. Consequently, the intermediate-state phase evolution and interferences between interfering ionization paths are approximately taken into account. Electron correlations play also an important role in the final state of the two-electron continuum and can strongly influence the momenta of the outgoing electrons. Most prominently, the repulsive electron-electron interaction suppresses the electrons ejected with momentum vectors pointing in the same direction. Final-state electron correlations can be accounted for by the exact double-continuum wave function. They are, however, absent in the (semi)analytical models for TPDI referred to above. We denote in the following such correlations in the double continuum as dynamical final-state correlations. While the atomic structure information and, consequently, static correlations are, thus, at least partially accounted for, the obvious shortcoming of those models is the neglect of dynamical correlations in the two-electron continuum.

Deviations from the predictions of these models, in particular for the two-electron angular distribution, can therefore serve as sensitive measures for the influence of such dynamical final-state electron correlation. While the perturbative models predict uncorrelated dipolar angular distributions for each electron ($\propto \cos^2\theta_1 \cos^2\theta_2$, where $\theta_{1,2}$ are the polar angles of the emitted electrons), pronounced deviations from such a distribution have been observed in a large number of numerical calculations [19,20,29,52]. The first indirect experimental evidence has emerged from the recoil-ion spectrum [15] but direct measurements of the joint momentum distribution are still missing.

Multidifferential measurements of TPDI of helium have remained a challenge because of both the low TPDI cross section and the low photon flux and low repetition rates of XUV photon sources available up to now. As more powerful HHG- and FEL-based sources are expected to become available, it is of interest to explore possible protocols to measure dynamical electron-electron correlations in the two-electron continuum. The central question to be addressed is this: Which level of multidifferential resolution is required to uniquely identify correlation effects? Conversely, can integrated and, hence, more robust measures be identified that still carry unambiguous signatures of correlation effects?

In the present paper we compare results from our numerical TDSE approach [29,52,62] to exactly solve the problem with a semianalytical model, which can accurately predict total cross sections as well as photoelectron energy distributions (PEDs). The latter model serves as point of reference in order to identify dynamical correlation effects in the double continuum. We focus on the projected joint momentum distribution $P(k_{1z},k_{2z})$, where $\mathbf{k}_i$ $(i = 1,2)$ are the vectoral momenta of the ejected electrons and the transverse coordinates are integrated over. We also investigate measures that result from further integration over this two-dimensional distribution and which are expected to be more robust in the view of the expected low count rates and in the presence of strong background signals.

The plan of the present paper is as follows. In Sec. II we briefly review the two complementary theoretical methods employed, the numerical solution of the TDSE and the virtual sequential model (VSM) based on time-dependent second-order perturbation theory (TDPT2). Numerical results for the projected joint momentum distributions derived from both TDSE and VSM allowing for identification of correlation effects are presented in Sec. III. Integrated measures, mainly the emission asymmetry and the azimuthal angle correlation function, are discussed in Sec. IV, followed by concluding remarks in Sec. V. Atomic units are used unless stated otherwise.

II. THEORETICAL METHODS

In this section, we briefly review two complementary methods employed in our study of the joint momentum distribution of TPDI of helium. We compare and contrast the results of the numerical solution of the TDSE with those from the semianalytical VSM which is based on second-order perturbation theory and neglects dynamical final-state correlations.

In our TDSE approach [29,30,52,62] the wave function $\Psi(\mathbf{r}_1,\mathbf{r}_2,t)$ is expressed in terms of a time-dependent close-coupling (TDCC) expansion:

$$\Psi(\mathbf{r}_1,\mathbf{r}_2,t) = \sum_{L,M,l_1,l_2} \frac{R^{L,M}_{l_1,l_2}(r_1,r_2,t)}{r_1 r_2} Y^{L,M}_{l_1,l_2}(\hat{r}_1,\hat{r}_2), \tag{1}$$

where

$$Y^{L,M}_{l_1,l_2}(\hat{r}_1,\hat{r}_2) = \sum_{m_1,m_2} \langle l_1 m_1 l_2 m_2 | l_1 l_2 L M\rangle Y_{l_1 m_1}(\hat{r}_1) Y_{l_2 m_2}(\hat{r}_2) \tag{2}$$

are the coupled two-particle spherical harmonics and $\langle l_1 m_1 l_2 m_2 | l_1 l_2 L M\rangle$ are the Clebsch-Gordan coefficients. For linearly polarized laser light, the magnetic quantum number $M = 0$ is conserved for double ionization from the ground state of helium. The radial part of the wave function is discretized by the finite-element discrete variable representation (FEDVR) method [63–65]. We use the Lanczos algorithm [66–69] for the time propagation. We extract information on the final state of the two-electron wave packet formed by the XUV pulse by propagating the wave function for a period of time after the conclusion of the laser pulse sufficiently long as to reach convergence [29]. We then project the wave function onto the product of two hydrogenlike scattering states of He^+:

$$f(\mathbf{k}_1,\mathbf{k}_2) = \langle \Psi_{\mathbf{k}_1}(\mathbf{r}_1)\Psi_{\mathbf{k}_2}(\mathbf{r}_2) | \Psi(\mathbf{r}_1,\mathbf{r}_2,t_f)\rangle. \tag{3}$$

The one-electron scattering state normalized in the momentum space is given by

$$\Psi_{\mathbf{k}}(\mathbf{r}) = \frac{1}{k}\frac{1}{\sqrt{2\pi}} \sum_{l,m} i^l e^{-i(\sigma_l+\delta_l)} Y^*_{lm}(\hat{k}) R_{kl}(r) Y_{lm}(\hat{r}), \tag{4}$$

where $\sigma_l = \arg\Gamma(l+1-i\frac{Z}{k})$ is the Coulomb phase shift, Z is the nuclear charge, and δ_l is the lth partial wave phase shift (with respect to the Coulomb waves) due to any non-Coulomb short-range admixture to the potential. In the present case, $Z = 2$ and $\delta_l = 0$. The radial wave function $R_{kl}(r)$ is analytically given by

$$R_{kl}(r) = \frac{2}{r}\frac{2^l e^{\pi Z/2k}|\Gamma(l+1-iZ/k)|}{(2l+1)!} e^{-ikr}(kr)^{(l+1)} \times {}_1F_1(l+1+iZ/k, 2l+2, 2ikr) \tag{5}$$

and is normalized as

$$\int_0^\infty r^2 R_{k'l}(r) R_{kl}(r)\, dr = 2\pi\delta(k-k'). \tag{6}$$

In Eq. (5) the Kummer confluent hypergeometric function is denoted by ${}_1F_1$. Inserting Eqs. (1) and (4) into Eq. (3), we obtain

$$f(\mathbf{k}_1,\mathbf{k}_2) = \frac{1}{2\pi k_1 k_2} \sum_{L,l_1,l_2} Y^L_{l_1,l_2}(\hat{k}_1,\hat{k}_2) M^L_{l_1,l_2}(k_1,k_2), \tag{7}$$

with

$$M^L_{l_1,l_2}(k_1,k_2) = (-i)^{l_1+l_2} e^{i[\sigma_{l_1}(k_1)+\sigma_{l_2}(k_2)]} \iint dr_1 dr_2 \times r_1 r_2 R_{k_1 l_1}(r_1) R_{k_2 l_2}(r_2) \Psi^L_{l_1,l_2}(r_1,r_2,t_f). \tag{8}$$

The fully differential vectorial joint momentum distribution of the two ejected electrons is now given by

$$P(\mathbf{k}_1,\mathbf{k}_2) = |f(\mathbf{k}_1,\mathbf{k}_2)|^2. \tag{9}$$

The projected (or reduced) joint momentum distribution along the laser polarization z axis follows as

$$P(k_{1z},k_{2z}) = \int P(\mathbf{k}_1,\mathbf{k}_2)dk_{1x}dk_{1y}dk_{2x}dk_{2y}. \quad (10)$$

Exploiting the azimuthal symmetry of Eq. (9), Eq. (10) can be reduced to a triple integral

$$P(k_{1z},k_{2z}) = 2\pi \int_{|k_{2z}|}^{\infty}\int_{|k_{1z}|}^{\infty}\int_0^{2\pi} k_1 k_2 \times P\left(k_1, \arccos\frac{k_{1z}}{k_1}, 0, k_2, \arccos\frac{k_{2z}}{k_2}, \Delta\phi\right) \times d\Delta\phi\, dk_1\, dk_2 \quad (11)$$

with $\Delta\phi = \phi_2 - \phi_1$ the difference between the azimuthal angles of the two emitted electrons.

Equations (9) and (11) can be alternatively calculated from TDPT2. Details can be found in Refs. [16,22–25,48–50,55]. In brief, the TPDI process is approximated by two one-photon single-ionization processes, the ionization of the neutral helium, $\mathrm{He} \rightarrow \mathrm{He}^+$, followed by photon ionization of the intermediate singly charged ionic state, He^+ to He^{2+}. Accordingly, dynamical electron correlations between the two outgoing electrons are neglected from the outset. In each separate transition the dipole matrix element couples the initial s state and the final p state, each of which gives the photoelectron distributions as $\propto \cos^2\theta$.

In the present implementation of the virtual sequential model as one variant of TDPT2, the fully differential probability is given by [22–25,49,50]

$$P(\mathbf{k}_1,\mathbf{k}_2) = \left(\frac{3}{4\pi}\right)^2 \frac{P(k_1,k_2)}{{k_1}^2{k_2}^2}\cos^2\theta_1\cos^2\theta_2 \quad (12)$$

with

$$P(k_1,k_2) = k_1k_2\frac{1}{2}\left(\frac{c}{4\pi^2}\right)^2 \left|\sqrt{\frac{\sigma^{\mathrm{He}}(E_1)}{\omega_{ai}}}\sqrt{\frac{\sigma^{\mathrm{He}^+}(E_2)}{\omega_{fa}}}K(E_a) + \sqrt{\frac{\sigma^{\mathrm{He}}(E_2)}{\omega_{bi}}}\sqrt{\frac{\sigma^{\mathrm{He}^+}(E_1)}{\omega_{fb}}}K(E_b)\right|^2, \quad (13)$$

where E_1 and E_2 are the energies of the two electrons, c is the speed of light, $\sigma^{\mathrm{He}}(E)$ and $\sigma^{\mathrm{He}^+}(E)$ are the one-photon single-ionization cross section of He and He^+, respectively, $\omega_{ai} = E_a - E_i$, $\omega_{fa} = E_f - E_a$, $\omega_{bi} = E_b - E_i$, $\omega_{fb} = E_f - E_b$, $E_i \approx -2.9037$ a.u., $E_a = E_1 - 2$ a.u., $E_b = E_2 - 2$ a.u., and $E_f = E_1 + E_2$. The so-called shape function $K(E_a)$ [16,22–25] is given by

$$K(E_a) = \int_{-\infty}^{\infty} d\tau_1 F(\tau_1) e^{i\omega_{fa}\tau_1}\int_{-\infty}^{\tau_1} d\tau_2 F(\tau_2) e^{i\omega_{ai}\tau_2}, \quad (14)$$

where $F(t)$ is the electric field of the laser pulse. $K(E_b)$ follows from Eq. (14), replacing the index a by b. $K(E_a)$ contains the spectral information on the initial (E_i) and intermediate state (E_a), the spectral broadening through the Fourier spectrum of the pulse, $F(t)$, as well as time ordering of the two single-ionization events ($|i\rangle \rightarrow |a\rangle \rightarrow |f\rangle$).

Inserting Eq. (12) into Eq. (11) yields the prediction for the projected joint momentum distribution:

$$P(k_{1z},k_{2z}) = \frac{9}{4}k_{z1}^2k_{z2}^2\int_{|k_{2z}|}^{\infty}\int_{|k_{1z}|}^{\infty}\frac{P(k_1,k_2)}{{k_1}^3{k_2}^3}dk_1\,dk_2. \quad (15)$$

III. NUMERICAL RESULTS FOR THE JOINT MOMENTUM DISTRIBUTION

We now compare numerical results for the projected joint momentum distribution along the polarization axis from the TDSE and TDPT2. This observable has in the past provided valuable experimental information on correlated two-electron emission by near-infrared strong field lasers [7,9]. It is expected to be experimentally accessible for the two-photon XUV photoionization in the near future. We consider photon energies ranging from 42 eV, deep in the nonsequential regime, to energies just above the threshold in the sequential regime at 54.4 eV.

The evolution of $P(k_{1z},k_{2z})$ as a function of photon energy is displayed in Fig. 1. At 56 eV, just above the threshold for sequential ionization, the two models are in near-perfect agreement. The spectral width of the 4-fs $\sin^2$ envelope pulse is sufficiently narrow ($\sim$1.5 eV) to avoid significant spectral overlap with the nonsequential regime. Obviously, in the sequential regime and for sufficiently long pulses dynamical correlation effects in the double continuum are largely negligible. The joint momentum distribution shows a pronounced twofold mirror symmetry ($k_{1z} \rightarrow -k_{1z}, k_{2z} \rightarrow -k_{2z}$) and the nodal planes ($k_{1z} = 0$, $k_{2z} = 0$) of the two "independent" dipolar emission patterns are well preserved. They cut into each of the four peaks of the crosslike pattern, giving rise to double peaks. Each double peak signifies the preferred extremely asymmetric energy distribution where one electron carries away almost the entire excess energy. Just below the threshold at 53 eV the first subtle effects of correlation become visible. While in the TDPT2 model the twofold mirror symmetry is strictly preserved, in the full TDSE calculation the lobes of the double peak lying in the second and fourth quadrants begin to be enhanced while the ones in the first and third quadrants are suppressed. This structure is closely related to the double-peak structure in the recoil momentum spectrum discussed by Kurka *et al.* for photon energies near 52 eV [15]. While in two theoretical simulations presented in Ref. [15] such a double-peak structure appeared, the corresponding experimental recoil distribution featured only a single broadened peak.

The mapping of the double peak in $P(k_{1z},k_{2z})$ onto the recoil momentum distribution is straightforward: the stronger lobe in the second and fourth quadrants corresponds to back-to-back emission of one fast and one slow electron, yielding a somewhat lower total recoil momentum, while the weaker lobe in the first and third quadrants corresponds to side-by-side emission of the electron pair with a similar asymmetric energy sharing, giving rise to a slightly larger recoil momentum of the He^{2+} nucleus. In a model without dynamical final-state correlation (such as the present version of TDPT2), both lobes have identical weight. The structural similarity of $P(k_{1z},k_{2z})$ just above and below the threshold, despite the marked quantitative differences, supports the notion of the "virtual"

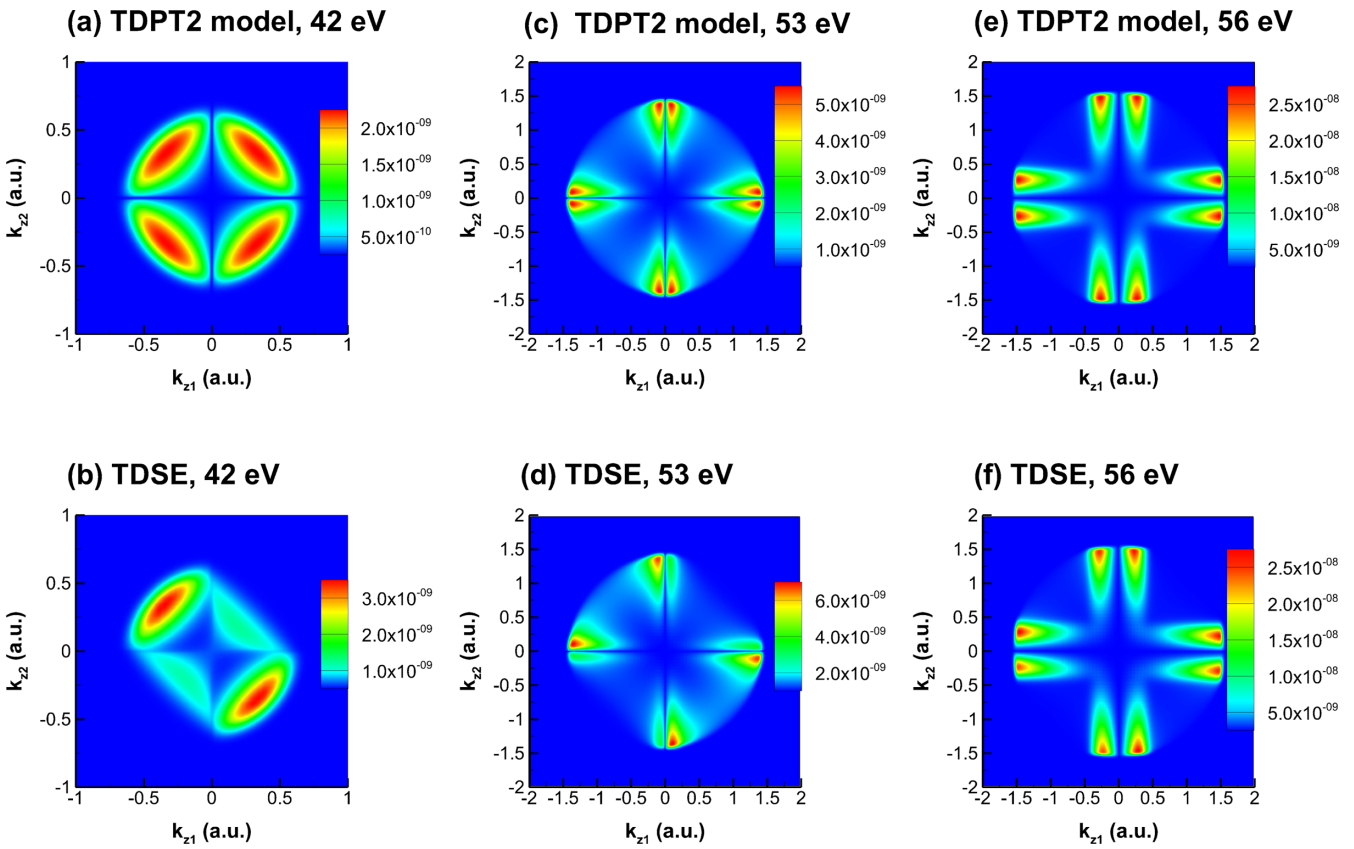

FIG. 1. The projected joint momentum distribution [see Eq. (10)] along the laser polarization axis at photon energies of (a), (b) 42 eV, (c), (d) 53 eV, and (e), (f) 56 eV. (a), (c), (e) Prediction from an uncorrelated VSM based on second-order time-dependent perturbation theory (TDPT2). (b), (d), (f) Prediction from the TDSE. In both cases, a 4-fs sine-squared-shaped laser pulse is used.

sequential ionization process put forward in Refs. [22–24]. The present analysis suggests that future measurement of $P(k_{1z},k_{2z})$ could help to resolve the discrepancy between theory and experiment for the recoil ion spectrum.

Lowering the photon energy further deep into the nonsequential regime (42 eV), the twofold symmetry is strongly broken. Emission takes place almost exclusively back-to-back (second and fourth quadrants) while side-by-side emission (first and third quadrants) is strongly suppressed. The TDPT2 model obviously fails to reproduce this effect. Moreover, the nodal planes of two separate dipolar emission processes predicted by this model are now largely smeared out in the TDSE solution. By comparing the joint momentum distribution at 42 and 52 eV it is obvious that the single broad peak for symmetric energy sharing ($k_z = -k_1 \approx 0.35$) at 42 eV results from merging of the two lobes of asymmetric energy sharing lying in the same quadrant (e.g., $k_{2z} = 1.35$, $k_{1z} = -0.15$ and $k_{2z} = 0.15$, $k_{1z} = -1.35$ in the second quadrant) as the photon energy is lowered. It has been shown previously that the present TDPT2 model can reliably reproduce total double-ionization cross sections as well as singly differential energy spectra [49,50], indicating that the single-ionization states form the dominant (on- or off-shell) intermediate states. The present results demonstrate that the final-state joint momentum distribution is a very sensitive measure for dynamical final-state correlations which are absent in the TDPT2. Dynamical correlations in the double continuum appear, for relatively long pulses (4 fs), prominently only in the strictly nonsequential regime. For shorter pulses this clear separation breaks down. This is due to two competing effects: for very short pulses (a few hundred attoseconds) the temporal proximity between the two ionization events renders the notion of sequential ionization obsolete [29,30,70]. For somewhat longer pulses ($\sim$1 fs) the increased spectral width of the pulse leads to the simultaneous presence of frequency components both above and below the sequential threshold. This is illustrated in Fig. 2, where for the same mean photon energy ($\langle\omega\rangle = 56$ eV) the joint momentum distribution for the 1-fs pulse (bandwidth 6 eV) reflects already features of the nonsequential regime, in particular the breaking of the twofold mirror symmetry. On the other hand, further increasing the pulse duration from 4 to 8 fs (bandwidth 0.75 eV) leaves $P(k_{1z},k_{2z})$ essentially unchanged. This should facilitate its experimental observation with an FEL source as the typical durations of the pulses within an FEL pulse train are of the order of $\sim$10 fs and fluctuating. Deep in the nonsequential regime (mean energy 42 eV), $P(k_{1z},k_{2z})$ is, apart from Fourier broadening, insensitive to the variation of pulse duration between 1 and 8 fs.

IV. INTEGRAL MEASURES

In view of the still considerable challenge to experimentally resolve the two-dimensional distribution $P(k_{1z},k_{2z})$ it is of interest to inquire into simpler and more robust measures for

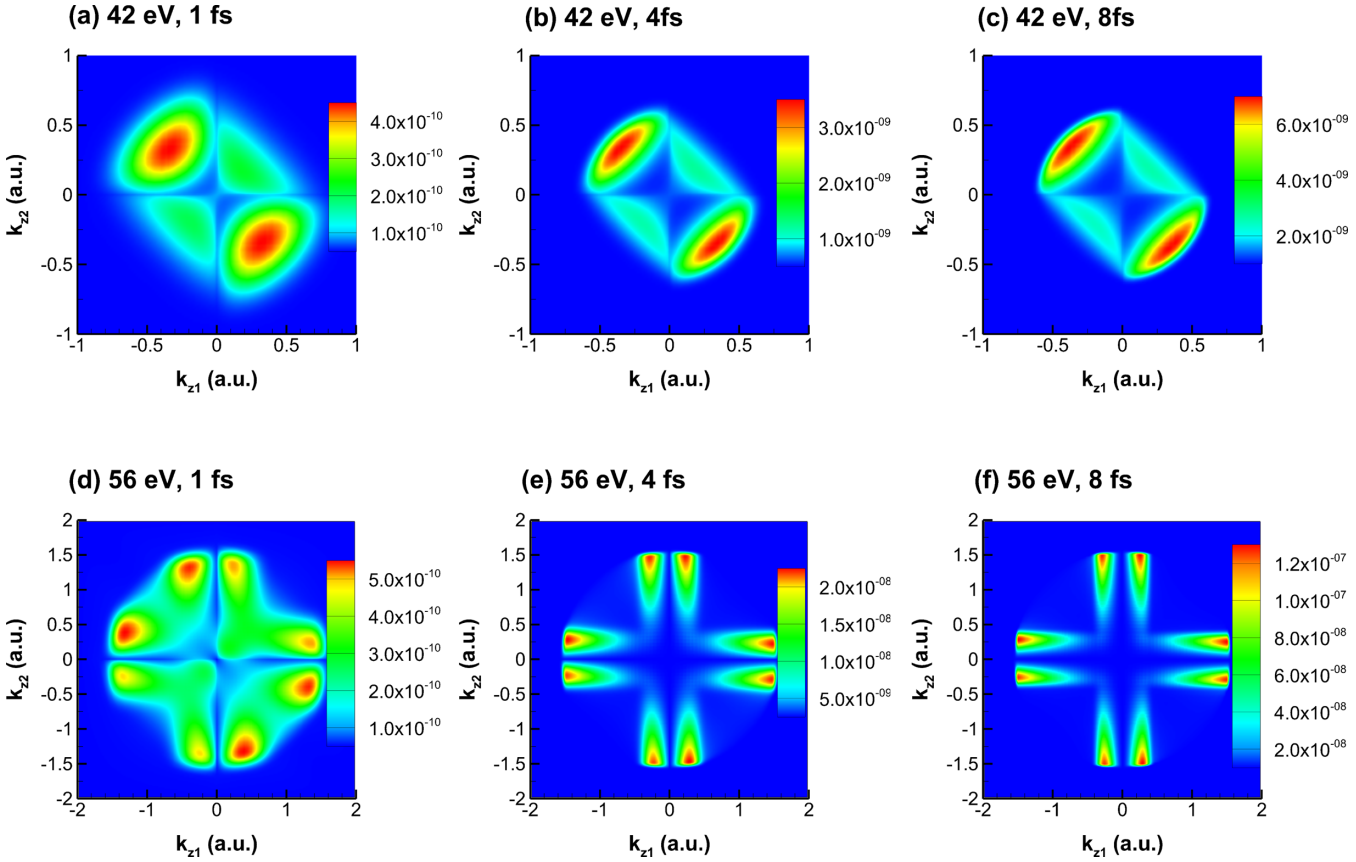

FIG. 2. Pulse duration dependence of the joint momentum distribution along the laser polarization axis (a)–(c) in the nonsequential regime and (d)–(f) in the sequential regime. Three pulse durations are compared: (a), (d) 1 fs, (b), (e) 4 fs, and (c), (f) 8 fs.

correlation effects that result from integration over the joint momentum distribution. We consider two such measures, the asymmetry A and the azimuthal correlation function $P(\Delta\phi)$. The asymmetry is defined in terms of integrals over selected quadrants of the joint momentum distribution function,

$$A = \frac{P(-,+) - P(+,+)}{P(-,+) + P(+,+)}, \tag{16}$$

where $P(+,+)$ is the integral over the first quadrant,

$$P(+,+) = \int_0^\infty dk_{1,z} \int_0^\infty dk_{2,z} P(k_{1,z},k_{2,z}), \tag{17}$$

representing (half of) the total side-by-side emission and

$$P(-,+) = \int_{-\infty}^0 dk_{1,z} \int_0^\infty dk_{2,z} P(k_{1,z},k_{2,z}) \tag{18}$$

is the corresponding integral over the second quadrant, giving the back-to-back emission. A similar but differential asymmetry parameter restricted to coplanar emission with fixed angle and energy sharing was introduced for quantifying the degree of (non)sequentiality [56]. The present asymmetry parameter [Eq. (16)] still requires coincident detection of two particles; however, only the sign of their longitudinal momentum component matters, irrespective of their energy and angular distribution. We therefore expect this parameter to be rather robust against noise from background signal present in the experiment with low (coincident) count rates.

From Fig. 1 it is obvious that A directly measures the degree of breaking of the twofold mirror symmetry and, thus, the dynamical final-state correlations in the two-electron emission process. Accordingly, A vanishes for all photon energies within the TDPT2 model (Fig. 3). By contrast, the full solution of the TDSE yields an asymmetry value of nearly 50% deep in the nonsequential regime while rapidly decaying near the

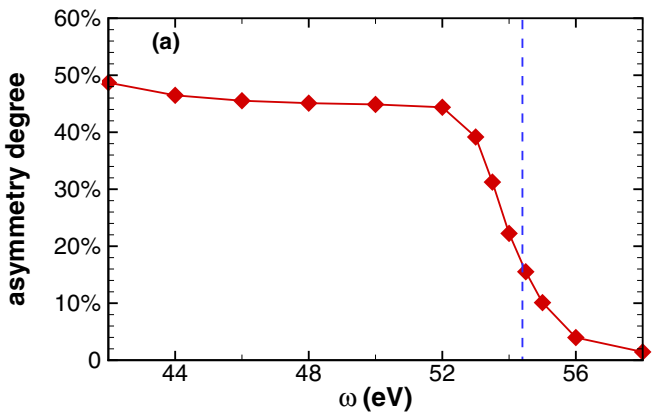

FIG. 3. Asymmetry A [Eq. (16); see the text for details] of the joint momentum distribution as a function of the photon energy. The pulse duration in the calculations is 4 fs. The VSM based on TDPT2 yields $A = 0$.

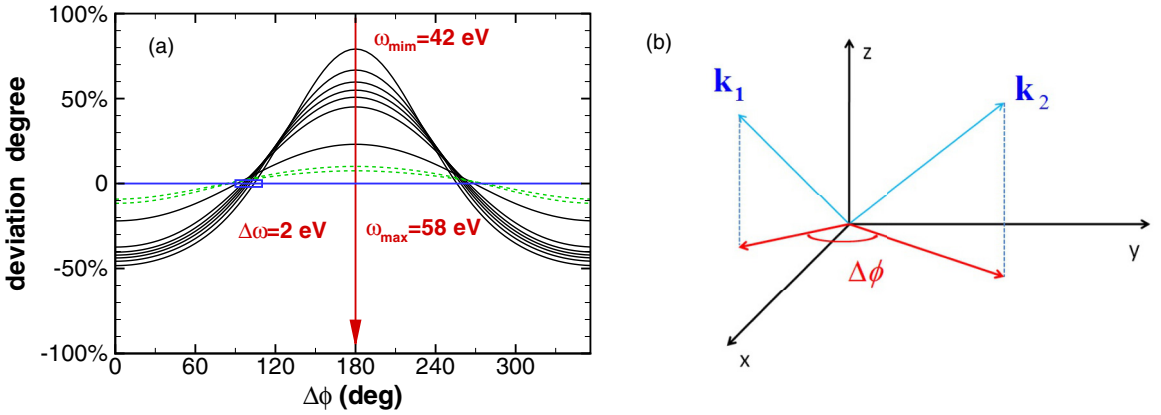

FIG. 4. Normalized variation of the azimuthal correlation function $P(\Delta\phi)$, $[P(\Delta\phi) - \langle P\rangle]/\langle P\rangle$ as a function of the azimuthal angle $\Delta\phi$ [defined in (b)]. The photon energies are varied between 42 and 58 eV in steps of 2 eV. Pulse duration is 4 fs. Solid black lines, energies below the threshold for sequential ionization; dashed green lines, energies above the threshold.

threshold to the sequential regime. The width of the transition region is governed by the spectral bandwidth of the XUV pulse. Well above the threshold and for sufficiently long pulse duration, A tends to zero, indicating that final-state correlations become unimportant.

As a second alternative integrated measure for dynamical correlations in the two-electron final state, we explore the azimuthal correlation function defined as (see Fig. 4)

$$P(\Delta\phi) = 2\pi \int\int\int\int k_1^2 k_2^2 \sin\theta_1 \sin\theta_2 dk_1 dk_2 d\theta_1 d\theta_2 \times P(k_1,\theta_1,0,k_2,\theta_2,\Delta\phi), \quad (19)$$

which measures the coincidence rate as a function of the difference $\Delta\phi = \phi_2 - \phi_1$ between the azimuthal angles of the two emitted electrons. In Eq. (19) both the energies (i.e., k_1 and k_2) and the polar angles of the two electrons are integrated over and need not be resolved. Figure 4(a) presents the variation of $P(\Delta\phi)$ normalized to its mean value, $[P(\Delta\phi) - \langle P\rangle]/\langle P\rangle$. This quantity vanishes identically for emission in the absence of angular correlation given by the TDPT2. For the full TDSE solution, by contrast, $P(\Delta\phi)$ reaches a peak value of $+80\%$ at $\Delta\phi = 180^\circ$ when the emitted electrons are farthest apart and is suppressed to $\sim -50\%$ when the electrons are emitted side-by-side. As a function of the photon energy the amplitude of the cosinelike variation of correlation function, monotonicity decreases and slowly approaches zero. Remarkably, for all energies, $P(\Delta\phi)$ coincides with $\langle P\rangle$ near $\Delta\phi = 100^\circ$. In view of the large contrast displayed by $P(\Delta\phi)$ this observable may become relatively easily accessible in future experiments with FEL and HHG sources.

V. SUMMARY

We have explored the joint momentum distribution projected along the polarization axis for two-electron emission in TPDI of helium. By employing both the full solution of the time-dependent Schrödinger equation and a model based on second-order perturbation theory we have identified features pinpointing dynamical electron correlations in the outgoing two-electron wave packet. The projected joint momentum distribution has been experimentally probed in strong-field ionization by IR pulses. We expect this distribution to be in reach for two-photon ionization with upcoming FEL and HHG sources. Moreover, we have introduced integrated measures, the asymmetry and the azimuthal correlation function, which might turn out to be more easily accessible and more robust in experimental settings with low count rates. Both observables provide sensitive measures for dynamical correlations in the double continuum as they yield nonzero values only when final-state correlations are accounted for. The present work suggests that such probes of correlations should be in reach at upcoming light sources, e.g., XFEL in Hamburg and ELI-ALPS in Szeged.

ACKNOWLEDGMENTS

We acknowledge helpful discussions with J. Feist and R. Pazourek. This work was supported by the FWF-SFB049(Nextlite) and FWF-SFB041(VICOM) funded by the Austrian Science Fund (FWF), and by the Natural Science Foundation of SZU (Grant No. 2017066). The computational results presented have been achieved using the Vienna Scientific Cluster (VSC).

[1] C. Bordas, F. Paulig, H. Helm, and D. Huestis, Rev. Sci. Instrum. **67**, 2257 (1996).
[2] R. Dörner, V. Mergel, O. Jagutzki, L. Spielberger, J. Ullrich, R. Moshammer, and H. Schmidt-Böcking, Phys. Rep. **330**, 95 (2000).
[3] T. Weber, H. Giessen, M. Weckenbrock, G. Urbasch, A. Staudte, L. Spielberger, O. Jagutzki, V. Mergel, M. Vollmer, and R. Dörner, Nature (London) **405**, 658 (2000).
[4] A. Rudenko, V. L. B. de Jesus, T. Ergler, K. Zrost, B. Feuerstein, C. D. Schröter, R. Moshammer, and J. Ullrich, Phys. Rev. Lett. **99**, 263003 (2007).
[5] X. Sun, M. Li, D. Ye, G. Xin, L. Fu, X. Xie, Y. Deng, C. Wu, J. Liu, Q. Gong, and Y. Liu, Phys. Rev. Lett. **113**, 103001 (2014).
[6] A. Staudte, C. Ruiz, M. Schöffler, S. Schössler, D. Zeidler, T. Weber, M. Meckel, D. M. Villeneuve, P. B. Corkum, A. Becker, and R. Dörner, Phys. Rev. Lett. **99**, 263002 (2007).

[7] B. Bergues, M. Kuebel, N. G. Johnson, B. Fischer, N. Camus, K. J. Betsch, O. Herrwerth, A. Senftleben, A. M. Sayler, T. Rathje, T. Pfeifer, I. Ben-Itzhak, R. R. Jones, G. G. Paulus, F. Krausz, R. Moshammer, J. Ullrich, and M. F. Kling, Nat. Commun. **3**, 813 (2012).

[8] Y. Liu, S. Tschuch, A. Rudenko, M. Dürr, M. Siegel, U. Morgner, R. Moshammer, and J. Ullrich, Phys. Rev. Lett. **101**, 053001 (2008).

[9] B. Wolter, M. G. Pullen, M. Baudisch, M. Sclafani, M. Hemmer, A. Senftleben, C. D. Schröter, J. Ullrich, R. Moshammer, and J. Biegert, Phys. Rev. X **5**, 021034 (2015).

[10] Z. Yuan, D. Ye, J. Liu, and L. Fu, Phys. Rev. A **93**, 063409 (2016).

[11] J. S. Prauzner-Bechcicki, K. Sacha, B. Eckhardt, and J. Zakrzewski, Phys. Rev. Lett. **98**, 203002 (2007).

[12] Y.-B. Li, X. Wang, B.-H. Yu, Q.-B. Tang, G.-H. Wang, and J.-G. Wan, Sci. Rep. **6**, 37413 (2016).

[13] C. Huang, M. Zhong, and Z. Wu, Opt. Express **24**, 28361 (2016).

[14] X. L. Hao, J. Chen, W. D. Li, B. Wang, X. Wang, and W. Becker, Phys. Rev. Lett. **112**, 073002 (2014).

[15] M. Kurka, J. Feist, D. A. Horner, A. Rudenko, Y. H. Jiang, K. U. Kühnel, L. Foucar, T. N. Rescigno, C. W. McCurdy, R. Pazourek, S. Nagele, M. Schulz, O. Herrwerth, M. Lezius, M. F. Kling, M. Schöffler, A. Belkacem, S. Düsterer, R. Treusch, B. I. Schneider, L. A. Collins, J. Burgdörfer, C. D. Schröter, R. Moshammer, and J. Ullrich, New J. Phys. **12**, 073035 (2010).

[16] K. L. Ishikawa and K. Midorikawa, Phys. Rev. A **72**, 013407 (2005).

[17] I. F. Barna, J. Wang, and J. Burgdörfer, Phys. Rev. A **73**, 023402 (2006).

[18] E. Foumoup, H. Bachau, and B. Piraux, Eur. Phys. J.: Spec. Top. **175**, 175 (2009).

[19] X. Guan, K. Bartschat, and B. I. Schneider, Phys. Rev. A **77**, 043421 (2008).

[20] S. X. Hu, J. Colgan, and L. A. Collins, J. Phys. B **38**, L35 (2005).

[21] K. Stefańska, F. Reynal, and H. Bachau, Phys. Rev. A **85**, 053405 (2012).

[22] D. A. Horner, F. Morales, T. N. Rescigno, F. Martín, and C. W. McCurdy, Phys. Rev. A **76**, 030701 (2007).

[23] D. A. Horner, C. W. McCurdy, and T. N. Rescigno, Phys. Rev. A **78**, 043416 (2008).

[24] D. A. Horner, T. N. Rescigno, and C. W. McCurdy, Phys. Rev. A **81**, 023410 (2010).

[25] A. Palacios, T. N. Rescigno, and C. W. McCurdy, Phys. Rev. A **79**, 033402 (2009).

[26] A. Palacios, D. A. Horner, T. N. Rescigno, and C. W. McCurdy, J. Phys. B **43**, 194003 (2010).

[27] R. Shakeshaft, Phys. Rev. A **76**, 063405 (2007).

[28] H. Bachau, Phys. Rev. A **83**, 033403 (2011).

[29] J. Feist, S. Nagele, R. Pazourek, E. Persson, B. I. Schneider, L. A. Collins, and J. Burgdörfer, Phys. Rev. A **77**, 043420 (2008).

[30] R. Pazourek, J. Feist, S. Nagele, E. Persson, B. I. Schneider, L. A. Collins, and J. Burgdörfer, Phys. Rev. A **83**, 053418 (2011).

[31] P. Lambropoulos, L. A. A. Nikolopoulos, M. G. Makris, and A. Mihelič, Phys. Rev. A **78**, 055402 (2008).

[32] J. Colgan and M. S. Pindzola, Phys. Rev. Lett. **88**, 173002 (2002).

[33] M. A. Kornberg and P. Lambropoulos, J. Phys. B **32**, L603 (1999).

[34] L. Malegat, H. Bachau, B. Piraux, and F. Reynal, J. Phys. B **45**, 175601 (2012).

[35] O. Chuluunbaatar, H. Bachau, Y. V. Popov, B. Piraux, and K. Stefańska, Phys. Rev. A **81**, 063424 (2010).

[36] I. A. Ivanov and A. S. Kheifets, Phys. Rev. A **79**, 023409 (2009).

[37] P. Lambropoulos and L. A. A. Nikolopoulos, New J. Phys. **10**, 025012 (2008).

[38] E. Foumouo, P. Antoine, H. Bachau, and B. Piraux, New J. Phys. **10**, 025017 (2008).

[39] H. Bachau, E. Foumouo, P. Antoine, B. Piraux, O. Chuluunbaatar, Y. Popov, and R. Shakeshaft, J. Phys.: Conf. Ser. **212**, 012001 (2010).

[40] E. Foumouo, G. L. Kamta, G. Edah, and B. Piraux, Phys. Rev. A **74**, 063409 (2006).

[41] Y. Qiu, J.-Z. Tang, J. Burgdörfer, and J. Wang, Phys. Rev. A **57**, R1489 (1998).

[42] J. Feist, S. Nagele, R. Pazourek, E. Persson, B. I. Schneider, L. A. Collins, and J. Burgdörfer, Phys. Rev. Lett. **103**, 063002 (2009).

[43] E. Foumouo, P. Antoine, B. Piraux, L. Malegat, H. Bachau, and R. Shakeshaft, J. Phys. B **41**, 051001 (2008).

[44] H. Bachau and P. Lambropoulos, Phys. Rev. A **44**, R9 (1991).

[45] S. Laulan and H. Bachau, Phys. Rev. A **68**, 013409 (2003).

[46] S. Askeland, R. Nepstad, and M. Førre, Phys. Rev. A **85**, 035404 (2012).

[47] S. Fritzsche, A. N. Grum-Grzhimailo, E. V. Gryzlova, and N. M. Kabachnik, J. Phys. B **41**, 165601 (2008).

[48] M. Førre, S. Selstø, and R. Nepstad, Phys. Rev. Lett. **105**, 163001 (2010).

[49] W.-C. Jiang, J.-Y. Shan, Q. Gong, and L.-Y. Peng, Phys. Rev. Lett. **115**, 153002 (2015).

[50] W.-C. Jiang, W.-H. Xiong, T.-S. Zhu, L.-Y. Peng, and Q. Gong, J. Phys. B **47**, 091001 (2014).

[51] Y. Tong, W.-C. Jiang, P. Wu, and L.-Y. Peng, Chin. Phys. B **25**, 073202 (2016).

[52] W.-C. Jiang, L.-Y. Peng, W.-H. Xiong, and Q. Gong, Phys. Rev. A **88**, 023410 (2013).

[53] W.-C. Jiang, Y. Tong, Q. Gong, and L.-Y. Peng, Phys. Rev. A **89**, 043422 (2014).

[54] C. Yu and L. B. Madsen, Phys. Rev. A **94**, 053424 (2016).

[55] S. Selstø, X. Raynaud, A. S. Simonsen, and M. Førre, Phys. Rev. A **90**, 053412 (2014).

[56] A. Liu and U. Thumm, Phys. Rev. Lett. **115**, 183002 (2015).

[57] A. Rudenko, L. Foucar, M. Kurka, T. Ergler, K. U. Kühnel, Y. H. Jiang, A. Voitkiv, B. Najjari, A. Kheifets, S. Lüdemann, T. Havermeier, M. Smolarski, S. Schössler, K. Cole, M. Schöffler, R. Dörner, S. Düsterer, W. Li, B. Keitel, R. Treusch, M. Gensch, C. D. Schröter, R. Moshammer, and J. Ullrich, Phys. Rev. Lett. **101**, 073003 (2008).

[58] Y. Nabekawa, H. Hasegawa, E. J. Takahashi, and K. Midorikawa, Phys. Rev. Lett. **94**, 043001 (2005).

[59] A. A. Sorokin, M. Wellhöfer, S. V. Bobashev, K. Tiedtke, and M. Richter, Phys. Rev. A **75**, 051402 (2007).

[60] H. Hasegawa, E. J. Takahashi, Y. Nabekawa, K. L. Ishikawa, and K. Midorikawa, Phys. Rev. A **71**, 023407 (2005).

[61] B. Manschwetus, L. Rading, F. Campi, S. Maclot, H. Coudert-Alteirac, J. Lahl, H. Wikmark, P. Rudawski, C. M. Heyl, B. Farkas, T. Mohamed, A. L'Huillier, and P. Johnsson, Phys. Rev. A **93**, 061402 (2016).

[62] Z. Zhang, L.-Y. Peng, M.-H. Xu, A. F. Starace, T. Morishita, and Q. Gong, Phys. Rev. A **84**, 043409 (2011).
[63] T. N. Rescigno and C. W. McCurdy, Phys. Rev. A **62**, 032706 (2000).
[64] M. J. Rayson, Phys. Rev. E **76**, 026704 (2007).
[65] B. I. Schneider and L. A. Collins, J. Non-Cryst. Solids **351**, 1551 (2005).
[66] T. J. Park and J. C. Light, J. Chem. Phys. **85**, 5870 (1986).
[67] E. S. Smyth, J. S. Parker, and K. Taylor, Comput. Phys. Commun. **114**, 1 (1998).
[68] M. Hochbruck and C. Lubich, SIAM J. Numer. Anal. **34**, 1911 (1997).
[69] B. I. Schneider, X. Guan, and K. Bartschat, in *Concepts of Mathematical Physics in Chemistry: A Tribute to Frank E. Harris—Part B*, edited by J. R. Sabin and R. Cabrera-Trujillo, Advances in Quantum Chemistry Vol. 72 (Academic Press, New York, 2016), pp. 95–127.
[70] R. Pazourek, S. Nagele, and J. Burgdörfer, J. Phys. B **48**, 061002 (2015).